



Pharmaceutical nanotechnology

## Multi-modal detection of colon malignancy by NIR-tagged recognition polymers and ultrasound contrast agents



Meital Bloch<sup>a</sup>, Lauren Jablonowski<sup>b</sup>, Eylon Yavin<sup>a</sup>, Dorit Moradov<sup>a</sup>, Irena Djavsarov<sup>a</sup>, Abraham Nyska<sup>c</sup>, Margaret Wheatley<sup>b,\*\*</sup>, Abraham Rubinstein<sup>a,\*</sup>

<sup>a</sup> The Hebrew University of Jerusalem, Faculty of Medicine, The School of Pharmacy Institute for Drug Research, P.O. Box 12065, Jerusalem 91120, Israel

<sup>b</sup> Drexel University, School of Biomedical Engineering, Science & Health Systems, Philadelphia 19104, PA, USA

<sup>c</sup> Timrat 36576, Israel

## ARTICLE INFO

## Article history:

Received 12 September 2014

Accepted 27 November 2014

Available online 28 November 2014

## Keywords:

Colon cancer  
Real time diagnosis  
Cationized polyacrylamide  
Recognition peptide  
Ultrasound  
Microbubbles

## ABSTRACT

To increase colonoscopy capability to discriminate benign from malignant polyps, we suggest combining two imaging approaches based on targeted polymeric platforms. Water-soluble cationized polyacrylamide (CPAA) was tagged with the near infrared (NIR) dye IR-783-S-Ph-COOH to form Flu-CPAA. The recognition peptide VRPMPQLQ (reported to bind specifically to CRC tissues) was then conjugated with the Flu-CPAA to form Flu-CPAA-Pep which was then incorporated into echogenic microbubbles (MBs) made of polylactic acid (PLA) that are highly responsive to ultrasound. The ultimate design includes intravenous administration combined with local ultrasound and intra-colon inspection at the NIR range. In this proof of principle study PLA MBs were prepared by the double emulsion technique and loaded with several types of Flu-CPAA-Pep polymers. After insonation the submicron PLA fragments (SPF)-containing Flu-CPAA-Pep were examined *in vitro* for their ability to attach to colon cancer cells and *in vivo* (DMH induced rat model) for their ability to attach to colon malignant tissues and compared to the specific attachment of the free Flu-CPAA-Pep.

The generation of SPF-containing Flu-CPAA-Pep resulted in a tissue attachment similar to that of the free, unloaded Flu-CPAA-Pep. The addition of VRPMPQLQ to the polymeric backbone of the Flu-CPAA reduced cytotoxicity and improved the specific binding.

© 2014 Published by Elsevier B.V.

### 1. Introduction

Efficient screening and early detection of colorectal cancer (CRC) is crucial for successful medical treatment and patients' survival (Edwards et al., 2010). Among common screening modalities such as double contrast barium enema, computed tomography and fecal occult blood test (Jemal et al., 2010), colonoscopy remains the gold standard screening method for detecting CRC at early stage, primarily in the distinction between benign and malignant polyps (Amri et al., 2013). However, because flat or depressed polyps are difficult to detect (Hsiung et al., 2008), improving the resolution of detection modalities that will verify

and support the endoscopy observations is a pressing clinical need. This could be accomplished by targeting molecular events during early CRC stages (Janakiram and Rao, 2008). Typical examples of reasonable protein targets for identifying CRC with sufficient specificity include vascular endothelial growth factor (VEGF) and epidermal growth factor receptor (EGFR) and use of these CRC-related proteins has led to the development of the monoclonal antibody drugs (bevacizumab and cetuximab, respectively) (Tonini et al., 2007). Still, their role in early stage CRC prognosis was found to be limited (Lee et al., 2002). Blood tests for biomarkers such as carcinoembryonic antigen (CEA) and carbohydrate antigen 19-9 are not specific enough for early diagnosis and are used for monitoring CRC patients who have already been diagnosed and are being treated (Duffy, 2001; Goetz et al., 2010).

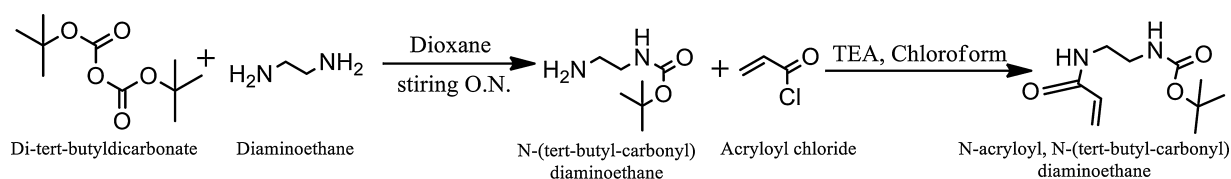
We have recently suggested that sialic acid could serve as a target for detecting CRC in the colon epithelium. Its identification was achieved by either fluorescently (FITC) tagged wheat germ agglutinin or cationized polyacrylamide (CPAA) (Azab et al., 2008). To enhance the recognition capabilities of the CPAA, the FITC was replaced with the indocyanine green derivative IR-783-S-Ph-COOH and the recognition peptide EPPT1 (specifically binds to the cell

**Abbreviations:** CPAA, cationized polyacrylamide; CRC, colorectal cancer; DMH, dimethyl hydrazine; Flu-CPAA-Pep, fluorescent-CPAA-peptide conjugate; IV, intravenous; MBs, microbubbles; NIR, near infrared; PLA, polylactic acid; SPF, submicron PLA fragments; US, ultrasound; UCA, ultrasound contrast agents.

\* Corresponding author. Tel.: +972 2 675 8603.

\*\* Corresponding author. Tel.: +1 215 895 2232.

E-mail addresses: [wheatley@coe.drexel.edu](mailto:wheatley@coe.drexel.edu) (M. Wheatley), [avrir@ekmd.huji.ac.il](mailto:avrir@ekmd.huji.ac.il) (A. Rubinstein).



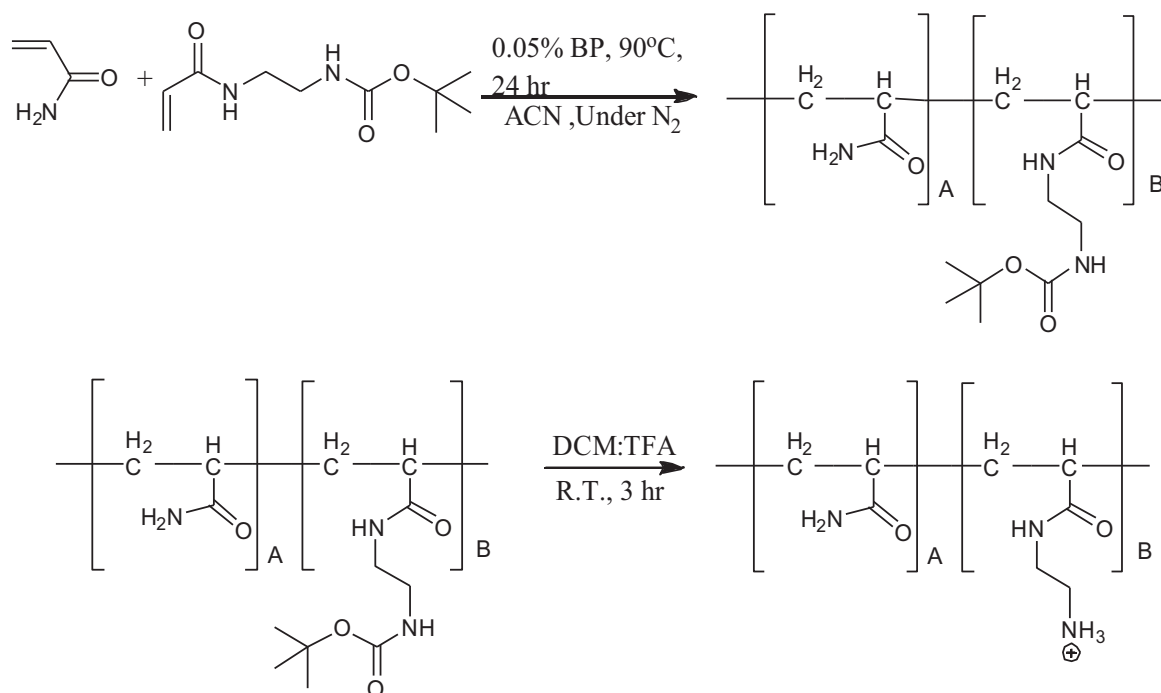
**Scheme 1.** Synthesis of the cationic monomer *N*-acryloyl, *N*-(tert-butyl-carbonyl)-diaminoethane.

transmembrane uMUC-1) was conjugated to the polymeric backbone to form Flu-CPAA-EPPT1. The use of short peptides as recognition tools is advantageous due to their ease of preparation at low cost, their negligible immunogenicity, their high affinity, and rapid binding kinetics (Kwon et al., 2012). The dual-recognition CPAA was tested successfully in colon cancer cells and in the orthotopic mouse model. It was concluded that the fluorescently-tagged CPAA could be used for the detection of malignant tissues in CRC after luminal instillation (Bloch et al., 2012). Based on molecular volume and reduced steric interference considerations with EPPT1, the present study employs a different recognition peptide, namely VRPMPLQ. After IV administration, VRPMPLQ showed selective binding to dysplastic tissue, although its molecular target was unknown and its sequence did not show full homology to ligands of known receptors (Hsiung et al., 2008).

To direct the Flu-CPAA-Pep to the region of interest in the colon a supportive technology is required. In the present study we tested the hypothesis that focused ultrasound (US) could be employed for that purpose. The use of US as a directing means, in both contrast imaging and drug delivery, depends on the echogenicity of the vehicle which determines its contrast properties. If properly designed, contrast US imaging allows real time anatomical imaging in the body (Anderson et al., 2011; Borden et al., 2008; Martínez-Rivas et al., 2010; Nicolau and Ripolles, 2012). Agent-enhanced US contrast is commonly achieved by creating gas-filled, stabilized microbubbles (MBs) that expand and contract in response to the oscillatory US pressure wave. At high acoustic pressures, MBs expansion and contraction leads to a phenomenon known as inertial or transient cavitation in which the bubbles rapidly expand through a few acoustic cycles to a radius of

over twice their initial size, followed by a violent collapse during the compression phase (Klibanov, 1999; Zhao et al., 2013). The ability of MBs to serve as efficient contrast agents depends on the gas compressibility, MBs dimensions, wall thickness, viscosity and density of the bubble shell as well as the intensity of the applied US field (Sirsi and Borden, 2009). The MBs dimensions should be in the order of magnitude of 1–6  $\mu\text{m}$  to allow for free passage through the vascular bed (Lentacker et al., 2006), while also allowing for greater effect from radiation force pushing the MB toward the vascular wall. Inertial cavitation and MBs fragmentation (required for penetrating the leaky malignant tissue (Cochran et al., 2011; Eisenbrey et al., 2010a) depend on the insonation parameters including frequency, intensity, and pulse repetition frequency as well as the size, composition and mode of MBs preparation that influence shell stiffness (Hernot and Klibanov, 2008; Zhao et al., 2013). Air-filled MBs made of poly lactic acid (PLA) showed good US contrast enhancement capabilities, smooth surface morphology, tight size distribution and, in the US beam, the ability to shatter into submicron fragments capable of escaping vascular pores, enabling cellular accumulation (Eisenbrey et al., 2010a,b). In contrast agents with more flexible shells this size reduction has been observed to be due to shriveling of the bubble caused by ultrasound-generation of a pore or rip in the shell with subsequent expulsion of the gas from the interior (Bouakaz et al., 2005).

Here we suggest a composite platform, made of the Flu-CPAA-Pep entrapped in the polymeric wall of echogenic MBs, for detecting malignant regions in the colon epithelium. As mentioned above, the selected recognition heptapeptide was VRPMPLQ. The ultimate plan is that following IV administration, the polymer-loaded MBs would



**Scheme 2.** Polymerization of CPAA-20 and CPAA-100.



**Table 1**

The increase in the fraction of amide bonds followed by the reduction of free amine groups as resulted by conjugating VRPMLPQ to Flu-CPAA-20 and Flu-CPAA-100 (each containing 4% of IR-783-Ph-S-COOH), as detected by XPS.

Probe	(%) N in C=ONH bond	(%) NH <sub>3</sub> <sup>+</sup>
CPAA-20	88.67	11.33
Flu-CPAA-20	90.06	9.94
Flu-CPAA-20 + 10% peptide	98.56	1.44
CPAA-100	66.34	33.66
Flu-CPAA-100	67.27	32.73
Flu-CPAA-100 + 10% peptide	79.99	20.01

in the DMH-induced rat model. The decision to create SPF in an *in vitro* acoustic setup prior to injection *in vivo* rather than generate them *in situ* in the animal was made in order to track only the behavior of the SPF, separate from the many other affects that US has on tissues *in vivo* (Qin et al., 2009) and to more closely match *in vitro* and *in vivo* SPF results.

## 2. Materials and methods

### 2.1. Materials

All materials were purchased from Sigma, St. Louis, MO, USA, unless otherwise stated. All solvents were analytical grade and were purchased from Bio Lab Jerusalem, Israel. Water was purified by reverse osmosis. Proton NMR was recorded on a 300 MHz Bruker NMR using deuterated solvents as internal standards. Mass analysis was performed by LCMS (Finnigan LCQ duo, ThermoQuest Corporation, CA, USA), Maldi-TOF (Voyager De Pro Applied Biosystems, CA, USA) and gel permeation chromatography (Multiangle laser light scattering, DAWN-F DSP Spectrophotometer, Wyatt, USA). Acryl amide and triethylsilane were purchased from Fluka, Switzerland; O-(7-azabenzotriazol-1-yl)-1,1,3,3-tetramethyluronium hexafluorophosphate (HATU) was purchased from Anaspec, Fremont, CA, USA; Benzoyl peroxide was purchased from Merck, Germany; Lutidine was purchased from ABCR GmbH, KG, Karlsruhe, Germany; PLA (100DL MW = 115 KDa) was purchased from Lakeshore Biomaterials Birmingham, AL, USA; poly(vinyl alcohol) (PVA) (88% mole hydrolyzed MW = 25 KDa) was purchased from Polysciences Warrington, PA, USA. All amino acids were purchased from Gl Biochem, Shanghai, China.

### 2.2. Cell lines

All cell lines, SW-620, HT-29, LS-174T and IEC-6 (a non-transformed rat small intestinal epithelial cell line with characteristics of crypt epithelial cells as control-low expression of sialic acid; do not express uMUC-1) were purchased from American Type Culture Collection, Manassas, Virginia, USA. While the human colon epithelium carcinoma cells HT-29 and LS-174T represent Stage B colon cancer severity (Duke staging system), SW-620 cells, were selected to represent Stage D, with increased expression of sialic acid (Azab et al., 2008). All cells were cultured (37 °C, 5% CO<sub>2</sub>), in DMEM medium supplemented with 10% fetal calf serum, 2 mM L-glutamine and 1% Pen/Strep solution (Beit Haemek, Israel). The IEC-6 cells were cultured as mentioned above with the addition of human recombinant insulin (1 U/ml) (Beit Haemek, Israel).

### 2.3. Animal studies

Male Sabra rats (200–250 g) were purchased from Harlan Laboratories, Israel. They were kept under controlled environmental conditions, (22 °C, 12 h light/dark cycles) and fed with standard

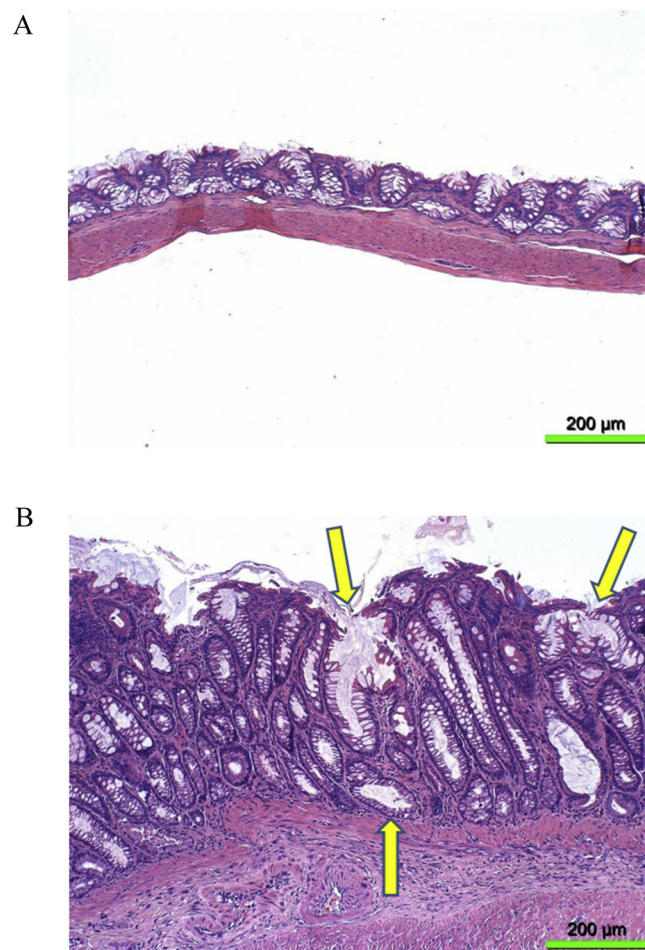


**Fig. 1.** Typical histological findings of specimens taken from the rat colon mucosa (magnification: 100×). (A) normal mucosa; (B) dysplasia. The dysplasia region is characterized by irregular crypt elongation and branching (arrows) associated with decreased goblet cell differentiation with basophilic cytoplasm and hyperchromatic nuclei. Multiple glands involved without distortion of adjacent mucosal architecture.

laboratory chow and tap water. The rat studies were conducted in accord with the Principles of Laboratory Animal Care (NIH publication #85-23, revised 1985). The joint ethics committee (IACUC) of the Hebrew University and Hadassah Medical Center for animal welfare approved the study protocol of the DMH induced rats. The Hebrew University Animal Facility is an AAALAC international accredited institute.

### 2.4. Methods

#### 2.4.1. Flu-CPAA-peptide synthesis

**2.4.1.1. Synthesis of N-acryloyl, N-(tert-butyl-carbonyl)-diaminoethane (the cationic monomer).** The BOC protected cationic monomer was prepared according to a previously published protocol (Scheme 1) (Bloch et al., 2012). The <sup>1</sup>H NMR (CDCl<sub>3</sub>) spectra were: <sup>1</sup>H: 1.435 (s, 9H, 3 × CH<sub>3</sub>), 3.318 (q, J = 5.7 Hz, 2H, CH<sub>2</sub>), 3.442 (m, 2H, CH<sub>2</sub>), 4.903 (s broad, <sup>1</sup>H, NH), 5.641 (dd, J = 10.2 Hz, J = 1.2 Hz, <sup>1</sup>H, CH<sub>2</sub> = CH), 6.087 (dd, J = 17.1 Hz, J = 10.2 Hz, <sup>1</sup>H, CH<sub>2</sub> = CH), 6.267 (dd, J = 17.1 Hz, J = 1.5 Hz, <sup>1</sup>H, CH<sub>2</sub> = CH), 6.395 (s broad, <sup>1</sup>H, NH). Electrospray ionization mass spectrometry (ESI-MS) (Thermo Scientific, San Jose, CA, USA) (+Na) was found to be: 236.9 g/mol (M<sub>calc</sub> = 214 g/mol). The yield averaged 84%.

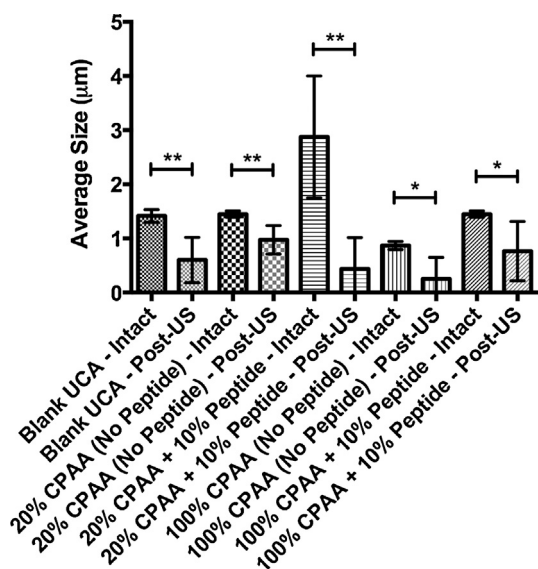


**Fig. 2.** Effect of the encapsulated polymers Flu-CPAA-20, Flu-CPAA-20-Pep, Flu-CPAA-100 and Flu-CPAA-100-Pep on the mean diameter of the PLA MBs before and after MBs sonication (UCA=MBs). Shown are the mean values of 3 different measurements  $\pm$  S.D. \* $p < 0.05$ ; \*\* $p < 0.025$ .

**2.4.1.2. Polymerization.** Two types of cationic polyacrylamide (CPAA), containing 20 (CPAA-20) or 100 (CPAA-100) mol% of the cationic monomer, were prepared as described previously (Bloch et al., 2012). After polymerization the tert-butyl-carbonyl protecting groups were removed by a 1:1 mixture of dichloromethane (DCM): trifluoroacetic acid (TFA) (Scheme 2).

The molecular weight of the two polymers was determined by gel permeation chromatography and was found to be in the range of 25–40 kDa.

**2.4.1.3. IR-783-S-Ph-COOH synthesis.** This IR-783 derivative was prepared as described previously (Bloch et al., 2012). The  $^1\text{H}$  NMR (CDCl<sub>3</sub>) spectra were:  $^1\text{H}$  NMR (CDCl<sub>3</sub>) 1H: 1.395 (s, 12H), 1.737 (m, 8H), 1.923 (m, 2H), 2.538 (overlap with DMSO, 4H), 2.768 (t, 4H,  $J =$

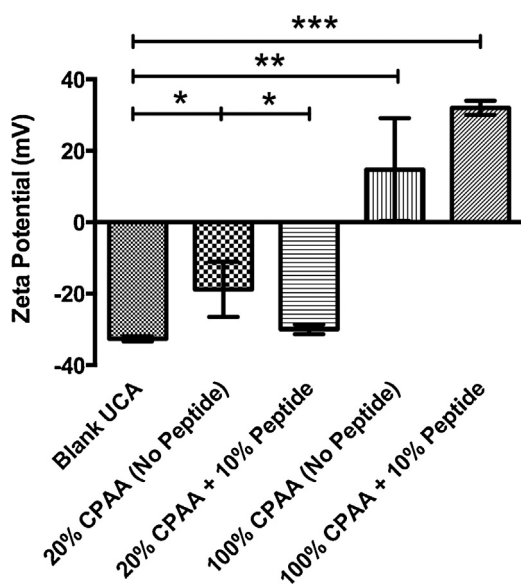


**Fig. 3.** Zeta potential of empty MBs and MBs loaded with Flu-CPAA-20, Flu-CPAA-20-Pep, Flu-CPAA-100 and Flu-CPAA-100-Pep. \* $p = 0.0181$  and  $0.0198$ , respectively, \*\* $p = 0.0023$ , \*\*\* $p < 0.0001$ . Shown are the mean values of 3 different measurements  $\pm$  S.D.

7.8 Hz), 4.149 (t, 4H,  $J = 7.8$  Hz), 6.353 (br d, 2H,  $J = 14.1$  Hz), 7.190 (dt, 4H,  $J = 2.4$  Hz,  $J = 7.5$  Hz), 7.383 (m, 4H), 7.496 (d, 2H,  $J = 7.5$  Hz), 7.771 (d, 2H,  $J = 8.4$  Hz), 8.595 (br d, 2H,  $J = 14.1$  Hz). The molecular weight was assessed by MALDI-TOF (Applied Biosystems – Voyager-D PRO, USA) and found to be 845.3 g/mol.

**2.4.1.4. Tagging CPAA with IR-783-Ph-S-COOH.** CPAA-20 and CPAA-100 were each conjugated, with 4% molar ratio of IR-783-S-Ph-COOH to form IR-783-S-Ph-CONH-CPAA in a powder form, as described previously (Bloch et al., 2012) to obtain Flu-CPAA-20 or Flu-CPAA-100.

**2.4.1.5. Synthesis of the VRPMPLQ peptide.** The peptide (Scheme 3) was prepared using a solid phase peptide synthesis (SPPS). The labile acid resin was 2-chlorotrityl chloride, allowing a controlled release of the anchored amino acids by eluting TFA 2%. The VRPMPLQ was acetylated to form  $\text{CH}_3\text{CO-NH}_2$ -VRPMPLQ-COOH to prevent self-interaction during the activation step. The sequential conjugation of the amino acids was conducted with the aid of *N,N*-diisopropylethylamine (DIEA), the coupling reagent 2-(1H-7-azabenzotriazol-1-yl)-1,1,3,3-tetramethyluronium hexafluorophosphate methanaminium (HATU), hydroxybenzotriazole (HOBT) and 2,6-dimethylpyridine (Lutidine), 4 equivalents each. The acetylated peptide was prepared using protection groups that allowed a control over the conjugation process with the polymeric backbone. The peptide was cleaved from the resin with a mixture of 2% TFA in dichloromethane, precipitated with diethyl ether, purified by HPLC (Column: C<sub>18</sub>, 250 mm, UV detector adjusted to  $\lambda_{\text{em}} = 220$  nm; gradient eluting system: 0.1% TFA in water and acetonitrile; gradient rate: 0–80% acetonitrile over 115 min), dried and lyophilized. The MW of the most significant peak, which was determined by ESI-MS ESI was found to be 745.38 g/mol [ $(M + 2)/2$ ] (calculated  $M = 744.4$  g/mol). A linker (aminohexanoic acid) was attached to the carboxyl end of the VRPMPLQ to maintain an optimal orientation upon attachment to the CPAA backbone to enable optimal recognition of the target biomarker.

**2.4.1.6. Conjugating VRPMPLQ with the Flu-CPAA and removal of the protecting groups.** Flu-CPAA-20 and Flu-CPAA-100 were each conjugated with 10 mol% of VRPMPLQ in its protected form. DIEA, HATU, HOBT and lutidine (4 equivalents each) were mixed (3 min) with the lyophilized peptide powder dissolved in 400  $\mu\text{l}$  of DMF. The obtained solution was added dropwise to the aqueous solutions of either Flu-CPAA-20 or Flu-CPAA-100, stirred for 6 h in the dark, diluted with water and the DMF was evaporated. The remaining aqueous solutions were centrifuged (7 min, 4000 rpm), the supernatant collected and dialyzed (cut off 6–8 kDa) against water to remove unreacted reagents and lyophilized to obtain the Flu-CPAA-20-Pep and Flu-CPAA-100-Pep conjugates as dry powders (Scheme 4). Cleavage (deprotection) was conducted by mixing the polymeric product in a solution of 88:5:5:2 TFA:water:phenol:triethylsilane (4 ml each) for 8 h. Sedimentation was obtained by adding cold diethyl ether and the precipitant was centrifuged, washed with diethyl ether and separated. The ether was evaporated and water was removed by lyophilization.

Characterization of the conjugated product was conducted by  $^1\text{H}$  NMR to identify typical peaks at the aromatic region and fluorescence measurements at  $\lambda_{\text{em}} = 700$  nm (Odyssey Imaging System, LI-COR, Lincoln, NE, USA) to qualitatively assess the creation of the fluorescently-tagged polymer containing the peptide (Scheme 4). X-ray photoelectron spectroscopy (XPS) was used to verify conjugation (Xu et al., 2010) by assessing the reduction in the free amine groups, associated with the appearance of amide bonds (Table 1).

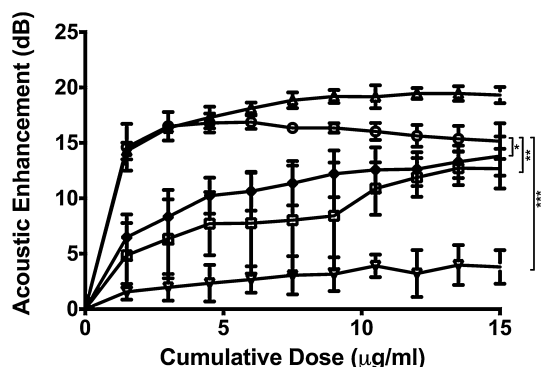


**Fig. 4.** Cumulative acoustic dose response curves of: -○- empty MBs and MBs loaded with -□- Flu-CPAA-20, -△- Flu-CPAA-20-Pep, -▽- Flu-CPAA-100, and -◆- Flu-CPAA-100-Pep. Shown are the mean values of 3 different measurements  $\pm$  S.D. \* $p$  = 0.0324, \*\* $p$  = 0.0032, \*\*\* $p$  < 0.0001.

#### 2.4.2. Preparation of CPAA loaded microbubbles (MBs)

Polymeric MBs containing the tagged targeting polymers were made of PLA, and prepared by an adaptation of the double emulsion w/o/w method described previously (Eisenbrey et al., 2010a). Briefly, the initial w/o emulsion was prepared by sonicating a mixture using dichloromethane as the organic phase containing the PLA, camphor as porogen and either Flu-CPAA-20, Flu-CPAA-20-Pep, Flu-CPAA-100, or Flu-CPAA-100-Pep and 0.4 M ammonium carbonate in deionized water as the second porogen in the initial water phase. This w/o emulsion was dispersed by homogenization into a large volume of 5% PVA forming the second emulsion. After evaporation of the organic phase and repeated washing, the hardening of the nascent capsules was achieved by washing with hexane. Hollow capsules were achieved by removal of remaining solvents and the porogens by lyophilization.

Size (expressed as peak % number), size distribution (as expressed by polydispersity index, PDI) and zeta potential of the MBs were measured (triplicates), after dispersing in water, on a Malvern Nano ZetaSizer (Worcestershire, UK) at room temperature. The concentrations of the various CPAA products in the MBs were determined by dissolving 1 mg of either loaded MBs or unloaded MBs (blank) in 1 ml of DMSO and measuring the fluorescent intensity at  $\lambda_{em} = 800$  nm and comparing values with a standard curve prepared in dimethyl sulfoxide (DMSO). Increasing amounts of Flu-CPAA-20, Flu-CPAA-20-Pep, Flu-CPAA-100 and Flu-CPAA-100-Pep in DMSO were used to establish a linear calibration curve for determining the encapsulation efficiency (EE), which was calculated according to Eq. (1):

$$EE(\%) = \left( \frac{W_1}{W_i} \right) \times 100 \quad (1)$$

where  $W_1$  is the weight of CPAA in the loaded MBs and  $W_i$  is the weight of the initial amount of the various CPAA probe used for loading. For all batches EE was found to be between 50 and 70%.

#### 2.4.3. Acoustic characterization: backscattering enhancement and MBs stability assessment

The *in vitro* acoustic testing setup was comprised of a transducer that was placed in a 37 °C water bath and focused through the acoustically transparent window of a custom-made plexiglas sample vessel containing 50 ml of PBS, pH 7.4. The transducer was connected to a pulser/receiver (model 5072 PR-Panametrics, Inc., Waltham, MA) to generate an acoustic pulse with a pulse repetition frequency (PRF) of 100 Hz. The reflected signal was detected with the same transducer, amplified to 40 dB by the pulser/receiver and then displayed on an oscilloscope (Lecroy 9350A, Chestnut Ridge, NY). The data was sent to a PC equipped with LabVIEW 7 Express (National Instruments, Austin, TX) that was used for data acquisition and processing (Cochran et al., 2011).

Incremental amounts (20  $\mu$ l) of MBs suspended in PBS (MBs concentration 3.75 mg/ml) were added to the acoustic vessel every 30 s over 5 min period, and their acoustic backscattering enhancement was recorded using the LabVIEW 7 programs, to create a dose response curve (10 points in triplicates).

The acoustic backscattering enhancement was defined by Eq. (2):

$$\text{Acoustic backscattering enhancement} = 20 \times \log \frac{\text{rms}_{\text{MBs}}}{\text{rms}_{\text{blank}}} \quad (2)$$

where  $\text{rms}_{\text{MBs}}$  and  $\text{rms}_{\text{blank}}$  are the root mean square values of 60 readings with MBs and the rms readings of 60 readings prior to MB injection, respectively, at the focus of the transducer (Cochran et al., 2011).

MBs stability in the US beam over time was assessed as follows: the sample vessel was filled with 50 ml of sterile PBS, pH 7.4 and mounted in the acoustic tank. The lowest amount of MBs that resulted in maximum echogenicity in the linear portion of the dose response curve (typically, 75–150  $\mu$ g MBs, based on the dose response curve) was introduced into the system and the acoustic enhancement of the MBs was recorded every 1 min over 15 min under continuous insonation. Results were expressed for dose response as enhancement in dB vs. dose, or for stability plots as normalized enhancement (with respect to initial reading) vs. time.

#### 2.4.4. Submicron PLA fragments (SPF)

**2.4.4.1. SPF analysis.** The SPF extravasation potential indicates the ability of the MBs to be fragmented by US. It is expected that, under US interrogation, the loaded MBs will rupture and result in sufficiently small particles that would be able to pass through the leaky vasculature of a tumor, while carrying the CPAA cargo. The appearance of submicron fragments was verified using Corning Transwell<sup>®</sup> inserts equipped with a polyester membrane with pores size of 400 nm which were placed in polystyrene 6 well plates containing 3 ml of PBS at 37 °C. Five milligram of polymer-loaded MBs were added to each well below the membrane. Inserts were modified with double sided tape to cover the side slits to allow for higher fluid levels, thus reducing the chances of creating a standing wave when insonated from the bottom. A rubber stopper was placed in the upper level of the liquid in each insert to act as an acoustic absorber to reduce reflections at the air–liquid interface that may also lead to a standing wave. The plate was then mounted on the water surface of a 37 °C water bath of the acoustic setup and

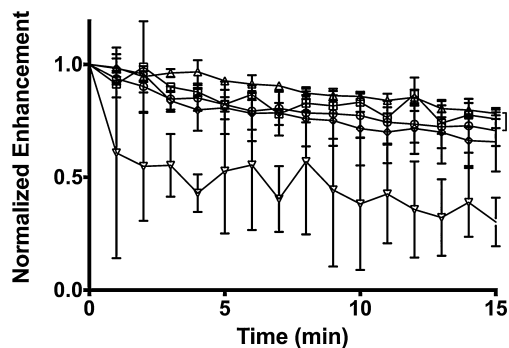


**Fig. 5.** Acoustic stability curves of empty -○- MBs and MBs loaded with -□- Flu-CPAA-20, -△- Flu-CPAA-20-Pep, -▽- Flu-CPAA-100, and -◆- Flu-CPAA-100-Pep. Shown are the mean values of 3 different measurements  $\pm$  S.D. \* $p$  = 0.0039, \* $p$  < 0.0001.

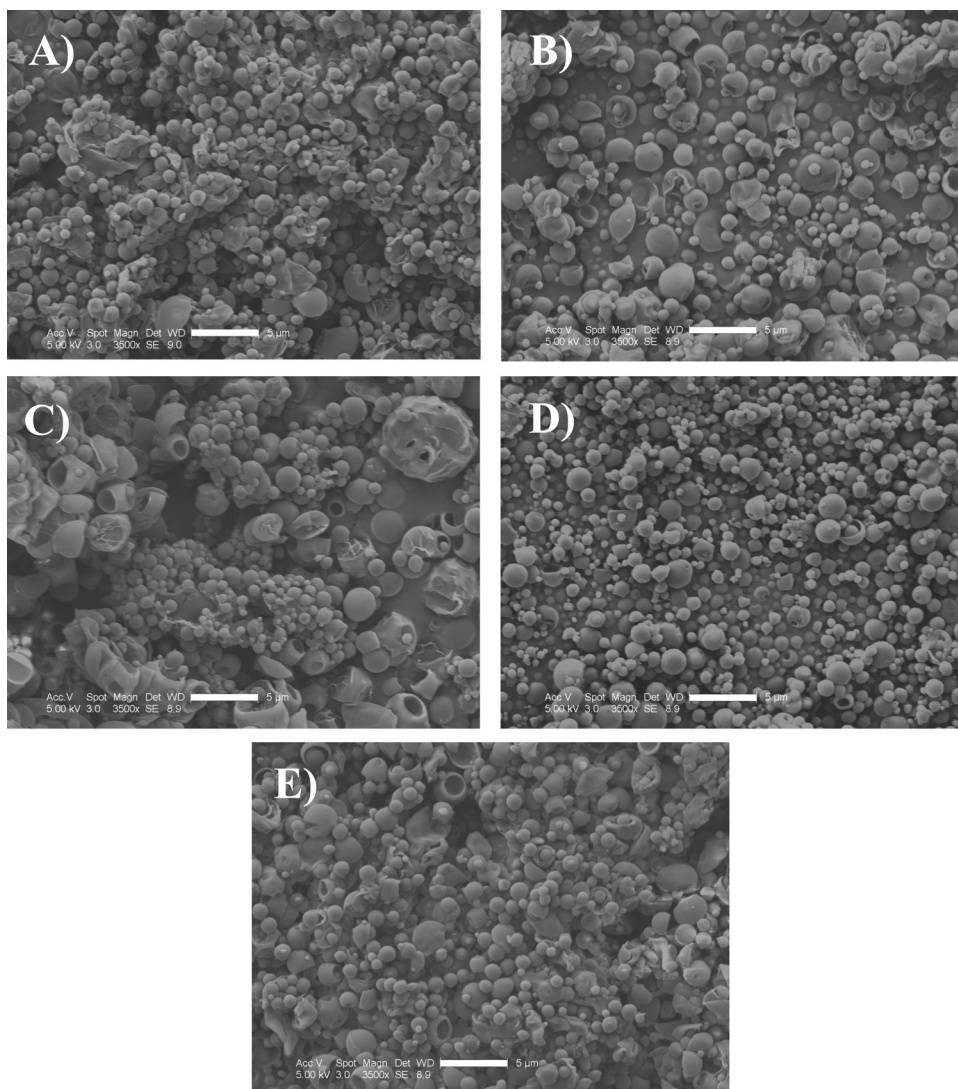


**Fig. 6.** Representative SEM micrographs of (A) unloaded MBs, (B) MBs containing Flu-CPAA-20, (C) MB containing Flu-CPAA-100, (D) MB containing Flu-CPAA-20-Pep and (E) MBs containing Flu-CPAA-100-Pep. Magnification: 3500 $\times$ ; Size bar = 5  $\mu$ m.

a 5 MHz transducer placed in the tank under the well was focused on the membrane of the insert which was then insonated for 30 min with a peak negative pressure of 0.94 MPa and a PRF of 5000 Hz (Cochran et al., 2011). Samples were withdrawn after passing the membrane filter immediately prior to insonation and at 5 min intervals over 30 min. with insonation. Each sample was lyophilized and its Flu-CPAA-Pep content were detected by measuring fluorescence intensity in the Odyssey Imaging System. Control studies included the same protocol on blank MBs and on experimental samples without insonation.

**2.4.4.2. Microscope analysis.** Images of the MBs, before and after insonation, were taken by an environmental scanning electron microscope (SEM) (Phillips FEI XL-30). Specimens (1 mg) were secured on aluminum stubs using a conductive double-sided tape and colloidal silver paint, and were then sputter coated with platinum-palladium at 40 mV for 40 s prior to imaging. The specimens were visualized under vacuum (upper limit of  $6.3 \times 10^{-6}$  mbar) and images were taken with beam excitation energy of 5 kV and a spot size of either 2 (high magnification, to reduce melting caused by the high imaging energy) or 3. After focusing, images were acquired and saved as high-definition TIFF files.

#### 2.4.5. Functional analysis in CRC cell lines

**2.4.5.1. Cytotoxicity assessment of SPF.** Cytotoxicity of aqueous extracts of SPF containing the Flu-CPAA-20, Flu-CPAA-100, Flu-CPAA-20-Pep and Flu-CPAA-100-Pep from the four types of insonated MBs was assessed by the MTT test (Hansen et al., 1989). Branched or linear polyethyleneimine (25 or 250 Kd, respectively) served as positive controls (high toxicity due to their positive charge), as well as sodium azide 10% w/v aqueous solution. The cells were grown in 24-well plates to 70% confluence. They were then divided into groups that were each incubated with 250  $\mu$ l of 1 mg/ml of each of the appropriate probes in triplicate. After 24 h the cells were washed ( $\times 3$ ) with PBS and 180  $\mu$ l of growth medium was added to each well followed by the addition of 20  $\mu$ l of 5 mg/ml MTT solution (final concentration of MTT in each well was 0.5 mg/ml). The plates were then incubated (37  $^{\circ}$ C, 5% CO<sub>2</sub>) for 2 h, the growth medium aspirated and replaced with 200  $\mu$ l of DMSO and incubated for an additional 40 min while shaking, at 37  $^{\circ}$ C. Absorbance was monitored on a microplate reader at 570 nm.

**2.4.5.2. In vitro cell binding.** The specific cell-binding of aqueous extracts (containing the SPF with Flu-CPAA-20, Flu-CPAA-20-Pep and Flu-CPAA-100-Pep) from the three types of SPF was assessed

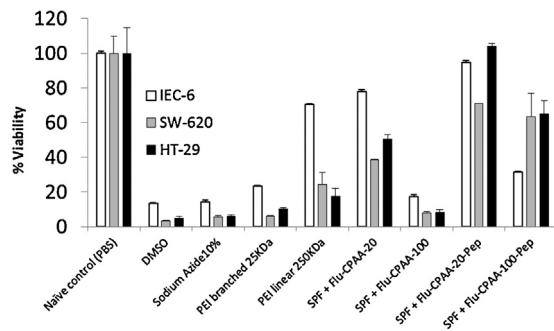


**Fig. 7.** Cytotoxicity of the SPF created from MBs containing Flu-CPAA-20, Flu-CPAA-100, Flu-CPAA-20-Pep and Flu-CPAA-100-Pep towards HT-29, SW-480, SW-620 and IEC-6 cells. Sodium azide, DMSO, linear and branched polyethyleneimine (PEI) served as positive controls. Shown are the mean values of 3 different studies in triplicates  $\pm$  S.D.

by monitoring the cells' fluorescence after 20 min incubation, as described previously (Bloch et al., 2012) and compared to the specific cell-binding of the non-loaded (free) polymer products as well as intact MBs. Briefly, cells were seeded on 96 well plates and grown to confluence. Prior to the experiment, the growth medium was aspirated and the cells were washed with PBS. 1 mg/ml in PBS of each probe was added to the cells and incubated (20 min, 37 °C) after which the cells were rinsed with PBS and the fluorescence was measured using the Odyssey Imaging System.

#### 2.4.6. DMH rat model

**2.4.6.1. In vivo tissue binding.** The experiments were conducted in Sabra rats treated with the carcinogen dimethylhydrazine (DMH) (LaMont and O'Gorman, 1978). Briefly, colon neoplasia was induced by a weekly subcutaneous injection of 100  $\mu$ l of DMH (4 mg/100 g rat body weight), for 5 weeks, after which the rats were kept for an additional 10 weeks, under daily inspection. SPF containing Flu-CPAA-20, CPAA-20-Pep, Flu-CPAA-100 and Flu-CPAA-100-Pep) from the four types of MBs, or non-loaded (free) CPAA products, were suspended in PBS and tested after rectal or IV administrations (500  $\mu$ l each). Twelve hours before the initiation of the rectal administration portion of the study, the rats were transferred to metabolic cages (with free access to water only) to ascertain empty colons. After anesthesia (a mixture of Ketamine and Xylazine HCl, 100 mg/kg rat body weight), aqueous dispersions (1 mg/ml) of the various probes were administered through a flexible, perforated Foley catheter. After 20 min, the colon of each anesthetized rat was rinsed ( $\times$ 3) with PBS. Three hours later the whole colons were exteriorized by laparotomy, cut open, spread on a polyethylene sheet with the mucosal aspect upwards and imaged by the Odyssey Imaging System, equipped with numeric quantification program, at  $\lambda_{em}$  = 800 nm. The anesthetized rats were sacrificed by chest wall puncturing (Bloch et al., 2012). Each polymer was tested in 5–6 DMH-induced rats. The fluorescence measurements were normalized to those obtained in the mucosa of the colons of non-treated (healthy) controls (2–3 control rats for each polymer product). In the IV administration portion of the study the aqueous dispersions of the above probes were injected into the tail vein of each rat (23 G needle). After 24 h the rats were anesthetized as described above, their whole colons were exteriorized and cut open, spread and imaged by the Odyssey Imaging System, as above. The anesthetized rats were then sacrificed.

**2.4.6.2. Histology analysis.** The extent of polymer-tissue binding was quantified by the intensity of the local fluorescence emission, expressed in arbitrary units (AU) at the regions of interest. Malignancy staging of the examined tissues was assessed

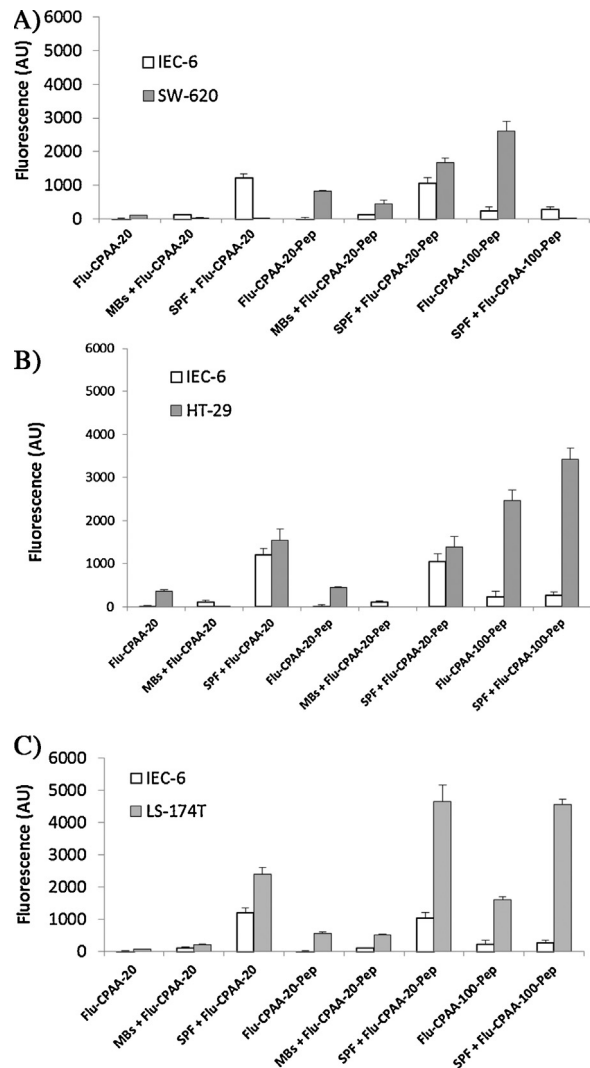


**Fig. 8.** The specific binding of Flu-CPAA-20, Flu-CPAA-20-Pep and Flu-CPAA-100-Pep free or in the form of MBs or SPF to, (A) SW-620, (B) HT-29 and (C) LS-174T colon cancer cells (filled columns) as expressed by cell fluorescence after 20 min incubation compared to the polymer binding to IEC-6 control cells (empty columns). Shown are the mean values of 3 different studies performed in triplicate  $\pm$  S.D.

histologically on specimens from polyps and adjacent tissues of each tested colon. The specimens were fixed in formaldehyde 4%. Slides were prepared by Patho-Lab Diagnostics (Ness-Ziona, Israel) and examined for colon cancer severity. Morphological analysis was conducted in accord with common criteria in the field (Fig. 1) (Elwell and McConnell, 1990; Newberne and Rogers, 1985; Whiteley et al., 1994).

#### 2.4.7. Statistical methods

Statistically significant differences for multiple groups were determined using a one-way ANOVA with a Newman-Keuls post test and individual groups were compared using a Student's *t* test. Statistical significance was determined using  $\alpha$  = 0.05. Error bars, where displayed, represent standard error of the mean.

### 3. Results

#### 3.1. Flu-CPAA conjugation into the MB

The average size of unloaded MBs in this study was  $1.42 \pm 0.07$   $\mu$ m, a size range that falls within the limits required

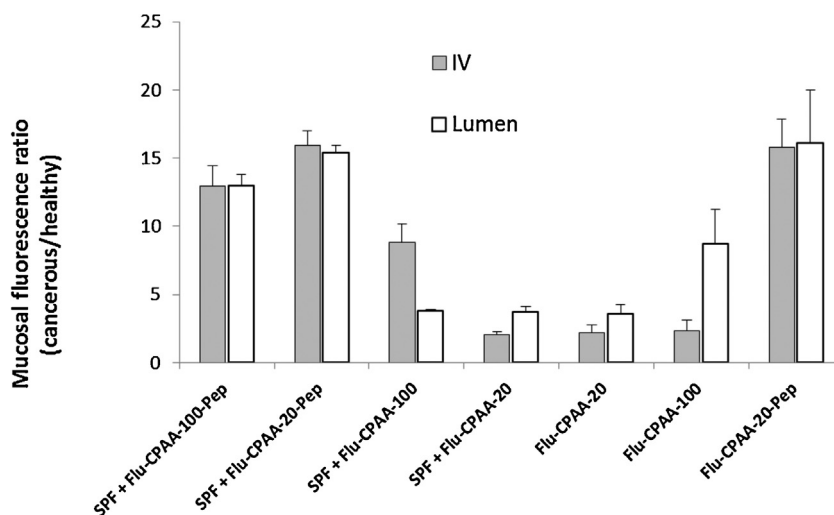


**Fig. 9.** The specific attachment of free Flu-CPAA-20, Flu-CPAA-20-Pep, Flu-CPAA-100 and Flu-CPAA-100-Pep or SPF, to malignant tissues of the DMH-induced rat after rectal (empty columns) or IV (filled columns) administration, as assessed by comparing the fluorescence in the tumor to the fluorescence in the adjacent healthy mucosal tissues (expressed in fluorescence ratio). Shown are the mean values of 5 different rat studies  $\pm$  S.D.

for free passage through the blood vessels and for SPF generation to occur under insonation (1–6  $\mu\text{m}$ ) (Quaia, 2007). Loading the MBs with Flu-CPAA-20 did not significantly change the dimensions of the MBs ( $1.45 \pm 0.03 \mu\text{m}$ ,  $p = 0.676$ ). However, Flu-CPAA-20-Pep increased the bubble size significantly ( $2.87 \pm 0.65 \mu\text{m}$ ,  $p = 0.0078$ ) and the Flu-CPAA-100 reduced the MB size significantly ( $0.87 \pm 0.04 \mu\text{m}$ ), values that are still within the size limits required for unimpeded passage through the vasculature and the creation of SPF (Fig. 2). Loading the MBs with Flu-CPAA-100 increased the MBs size distribution (polydispersity index (PDI) of unloaded bubbles =  $0.24 \pm 0.02$ , and PDI of MBs loaded with Flu-CPAA-100 =  $0.34 \pm 0.02$ ), while loading them with Flu-CPAA-100-Pep did not alter their average size ( $1.45 \pm 0.03 \mu\text{m}$ ) or the size distribution (PDI =  $0.28 \pm 0.03$ ). Similarly, incorporation of Flu-CPAA-20 had no significant effect on the PDI ( $0.28 \pm 0.03$ ). MBs loaded with the Flu-CPAA-20-Pep had a reduced PDI ( $0.13 \pm 0.05$ ). As expected, the US-driven SPF creation caused a profound reduction in the size of all the MBs (Fig. 2). The change in size of the MBs after their loading with Flu-CPAA-20 was accompanied by an increase in the zeta potential, from  $-32.6 \pm 0.4 \text{ mV}$  for unloaded MB to  $-18.8 \pm 4.4 \text{ mV}$  ( $p = 0.0181$ ), reflecting a reduction in the surface negative charge of the MBs due to the presence of the positive charge on Flu-CPAA-20 (Fig. 3). Flu-CPAA-100 and Flu-CPAA-100-Pep completely diminished the surface negative charge of the MBs, transposing the values to positive ( $14.7 \pm 8.3 \text{ mV}$  and  $32.0 \pm 1.2 \text{ mV}$ , respectively).

### 3.2. MB Acoustic characterization

The acoustic properties of the different CPAA-loaded MBs were assessed by examining (a) their ability to reflect US (echogenicity) (5 MHz) and (b) their stability under the US beam (5 MHz) over time. These experiments were used to assess the influence of CPAA loading on these acoustic properties of the various MBs. The echogenicity test was conducted in a dose–response manner to identify the optimal dose, where the US enhancement was maximal. The dose response curves (Fig. 4) indicate that encapsulation of the polymers had a profound and polymer-specific effect on the echogenic response. Flu-CPAA-100 essentially reduced the response to background, while Flu-CPAA-20-Pep removed shadowing (reduction of dB as dose increases past a maximum) at doses above 5  $\mu\text{g/ml}$ . Flu-CPAA-100-Pep and Flu-CPAA-20 had responses that lay between these extremes and were

not statistically different from each other. However, the fact that they had a very slow rise to a value that had not peaked at the highest measured dose of 15  $\mu\text{g/ml}$  indicates that many of the MBs were not echogenic in these samples.

The stability of the various types of MBs when exposed to the US beam was assessed by monitoring the acoustic backscattering enhancement values every minute over 15 min under continuous insonation. This gives a measure of their ability to act as US contrast agents during circulation and an estimate of the effect that incorporation of the various CPAA polymers had on the ability of the loaded MBs to break into SPF. The acoustic stability curves are shown in Fig. 5. Apart from MBs loaded with Flu-CPAA-100, the stability of all loaded MBs was not affected significantly compared to the unloaded MBs. This together with the poor dose response curve suggests that the Flu-CPAA-100 impacted the double emulsion method of MB generation in a different and adverse fashion, probably as a function of the higher cationic content of the polymer, without the benefit of shielding by the recognition peptide. SEM microphotographs of the various MBs are shown in Fig. 6.

### 3.3. SPF cytotoxicity assessment

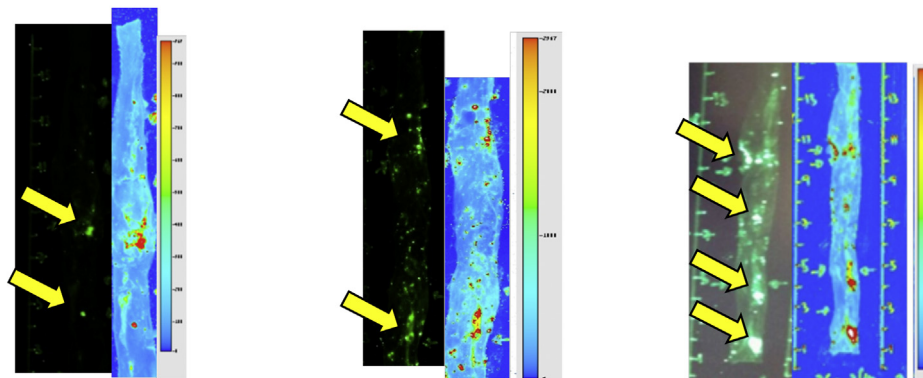
The cytotoxicity of the loaded SPF towards three different cell lines is summarized in Fig. 7. For each cell line cytotoxicity was in the order SPF-CPAA-100 >>> SPF-CPAA-20 > SPF-CPAA-100-Pep >> SPF-CPAA-20-Pep. The enhanced cytotoxicity of the fragments containing Flu-CPAA-100 compared to those containing Flu-CPAA-20 is most probably due to the higher amount of the cationic

**Table 2**

The fraction (in %) of specific attachment to dysplastic regions in the colonic mucosa of DMH-induced rats of SPF, containing Flu-CPAA-100, or Flu-CPAA-100-Pep or Flu-CPAA-20, or Flu-CPAA-20-Pep compared to adjacent healthy mucosal tissues, after intravenous (IV) or rectal administrations.

Extract	Mode of administration	Fraction attached (%)
SPF + Flu-CPAA-100-Pep	IV	80
SPF + Flu-CPAA-100-Pep	Rectal	100
SPF + Flu-CPAA-20-Pep	IV	60
SPF + Flu-CPAA-20-Pep	Rectal	50
SPF + Flu-CPAA-100	IV	100
SPF + Flu-CPAA-100	Rectal	75
SPF + Flu-CPAA-20	IV	100
SPF + Flu-CPAA-20	Rectal	50

### Rectal Administration

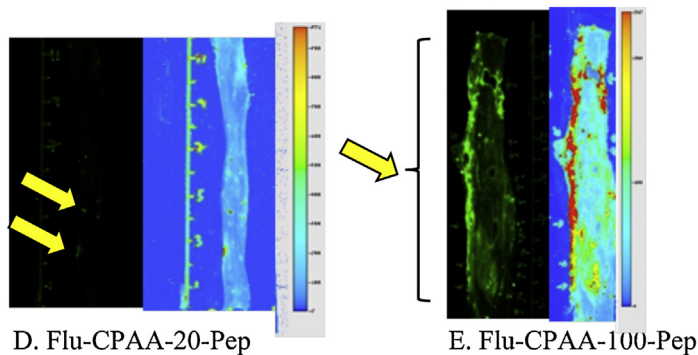


A. Flu-CPAA-100-Pep

B. Flu-CPAA-100-Pep

C. Flu-CPAA-20-Pep

### IV Administration



D. Flu-CPAA-20-Pep

E. Flu-CPAA-100-Pep

**Fig. 10.** Fluorescent images of dysplasia regions in the colonic mucosa of DMH induced rats after rectal (top row) or IV (low row) administration of suspended extracts of Flu-CPAA-100-Pep (A, B and E) and Flu-CPAA-20-Pep (C and D) taken from SPF. Left panels: Odyssey images (800 nm, intensity set to 2); Right panels: spectral analysis to regions of interest (ROI), analyzed by ASI computerized program of the Odyssey images, with a fluorescent intensity scale. Arrows: specific attachment of the Flu-CPAA-20-Pep or Flu-CPAA-100-Pep to the regions identified histologically as dysplasia.

monomer content in the polymer. Conjugating the recognition peptide VRPMLQ to the CPAA polymeric backbone reduced the cytotoxicity of the polymer-loaded SPF. The cytotoxicity towards the IEC-6 control cells emphasizes the importance of local delivery aspects of the technology.

#### 3.4. Cell attachment studies

The specific binding of the various Flu-CPAA products, with and without the affinity peptide, was compared to their binding after loading into the MBs and after the creation of SPF. MBs containing Flu-CPAA-100 were not included due to the relatively high cytotoxicity of the polymer (Fig. 7). The attachment results are summarized in Fig. 8, in which binding to SW-620, HT-29 and LS-174T is compared to binding to control cell line IEC-6. The results demonstrate the following: (a) binding is dependent on cell type. (b) While binding to control is low in most cases, binding of the SPF containing CPAA-20-Pep is noticeable. (c) Cellular attachment of SPF containing Flu-CPAA-20 MBs and Flu-CPAA-20-Pep MBs was greater than their respective intact MBs for all IEC-6, HT-29 and LS-174T cells;  $p < 0.05$  for all pairs. Additionally, these fragments exhibit greater attachment than their non-encapsulated controls;  $p < 0.05$  for all pairs. (d) Flu-CPAA-20 bound poorly in all cell lines (polymer, MB and SPF) except for SPF interacting with HT-29 and LS-174 (fluorescence AU of 1543.97 and 2401.54, respectively). (e) Addition of the peptide to give Flu-CPAA-20-Pep increased the binding compared to native polymer (Flu-CPAA-20) in all cases. (f) Flu-CPAA-100-Pep bound to all cell lines and the SPF were

superior to native polymer in all cases except SW-620, for which no binding was observed. (g) In all cases SPF binding was superior to MB binding except for SPF containing Flu-CPAA-100-Pep with SW-620 cells. (h) Binding of SPF containing Flu-CPAA-100-Pep to the cells was found to be superior over the rest of the fragmented MBs.

#### 3.5. Mucosal attachment in the colon of DMH-induced rats

The results of the *in vivo* binding experiments to the malignant tissues in the rat colon after intrarectal or IV administration of the SPF and free polymers are summarized in Fig. 9. The figure demonstrates that (a) conjugating the VRPMLQ recognition peptide to the Flu-CPAA backbone increased the specific binding to the cancerous regions in the rat colons for both CPAA-20 and CPAA-100, in both IV and rectal administrations; (b) the Flu-CPAA-20-Pep did not differ from the Flu-CPAA-100-Pep in terms of specific attachment to the cancerous tissues; and (c) except for the Flu-CPAA-100 (in the presence or absence of SPF), no profound difference could be observed in the attachment of the polymers after the IV and the rectal (luminal) administrations.

#### 3.6. Histological analysis and cancer stage-dependent attachment

The relationship between colon tissue fluorescence (caused by the specific attachment of the various Flu-CPAA products entrapped in SPF) and malignancy severity (staging by histological analysis) is summarized in Table 2. The results indicate that the Flu-CPAA products attached most profoundly to those regions

identified with dysplasia (Fig. 10), with the highest attachment observed with Flu-CPAA-100-Pep after both IV and rectal administration, suggesting that the optimal product for early diagnosis of CRC would be Flu-CPAA-100-Pep. Flu-CPAA-20-Pep on the other hand, was attached mostly to tissue identified with carcinoma (data not shown), indicating that Flu-CPAA-20-Pep could also be used for detecting more advanced stages of CRC.

#### 4. Discussion

In the present study, we prepared two types of cationic polyacrylamide (CPAA), CPAA-20 and CPAA-100, differing from each other by the content of the cationic monomer (20 and 100 mol %, respectively). By virtue of their positive charge, they were capable of attaching to typically negatively-charged mucinous regions in the vicinity of malignant tissues in the colon. Conjugation of a fluorophore tag, IR-783-S-Ph-COOH (an IR-783 derivative in the NIR range) to the polymeric backbone, *via* the appended NH<sub>2</sub> groups of the CPAA, created a Flu-CPAA with the assumed capability of identifying pre-malignant pathology in the colon epithelium with the aid of endoscopic means. The study also examined the question of whether conjugating the recognition peptide VRPMPLQ to these cationic polymers could improve their targeting capabilities in the colon. This peptide was selected due to its reported ability to detect colon carcinoma (Hsiung et al., 2008) and its relatively low molecular weight that would minimize the potential for steric hindrance that may happen during the recognition process (Bloch et al., 2012).

The suggested diagnosis tactics with the Flu-CPAA-Pep included IV administration of the tagged polymer, preferential accumulation at the target site and monitoring of the tissue fluorescence from the lumen aspect of the colon by an endoscope with fluorescence detection capabilities in the NIR range. To prevent premature protein binding of the targeting polymer after the IV administration, it was loaded into PLA MB that served as UCA designed to shatter into SPF when exposed to a focused US beam, directed at the region of interest in the colon. It has already been shown that US does not affect cargo molecules or polymers loaded into MBs (Endo-Takahashi et al., 2012; Lentacker et al., 2006).

Ideally, a targeted delivery system is expected to be able to carry its cargo while circulating in the blood stream and release it, solely, at the target site to create high local concentration. By using MB as the supportive delivery vehicle, the oscillation caused by the directed US is intended to fragment the MBs into nano sized particles, that will exit the vasculature and penetrate into the tumor (*e.g.*, dorsal aspect of a colon polyp) by a combination of radiation force and forces generated during degrading into SPF (Cochran et al., 2011). Localization of acoustic energy is possible into millimeter and even sub-millimeter volumes allowing precise spatial control of cargo discharge (Gao et al., 2008). The close proximity of the MBs to the vascular wall caused by the US radiation force will effectively promote the release of SPF containing the tagged polymer into the endothelium upon the rupture of the MB (Ferrara et al., 2007).

The Flu-CPAA products were loaded into the MBs during their fabrication by mixing them with the organic phase of the double emulsion system. This method is known to result in MBs within the desired size limit of 1–6 μm (Lentacker et al., 2006), with a doubling of the average diameter of the MBs containing Flu-CPAA-20-Pep ( $p = 0.045$ ) and a decrease in the average diameter of 61% in the MBs containing Flu-CPAA-100 ( $p = 0.0012$ ) compared to blank control MBs (Fig. 2). The average diameter of MBs containing Flu-CPAA-20 and Flu-CPAA-100-Pep did not differ significantly from the control unloaded MBs. The diameter and size distribution of MBs formed by the solvent/evaporation techniques are determined at the droplet formation steps. These two parameters are also

affected by the changes in viscosity brought about when the CPAA polymers are added to the system and reacted with the PLA. Furthermore, the presence of Flu-CPAA in the wall of the MBs had an effect on the zeta potential of the resulting bubbles. The zeta potential of the empty (blank) MBs ( $-32 \pm 0.4$  mV) reflects the negative charge on the PLA. The incorporation of Flu-CPAA-20, Flu-CPAA-100 and Flu-CPAA-100-Pep led to a gradual increase in the zeta potential as the proportion of positively charged -NH<sub>3</sub> groups increased. However, the zeta potential achieved by incorporation of Flu-CPAA-20-Pep did not follow this trend. We suggest that, in this case, the presence of VRPMPLQ on the Flu-CPAA-20 was enough to shield the overall positive charge contributed by the lower proportion (20 mol% vs. 100 mol%) of cationic monomer resulting in a negative zeta potential similar to that of the control unloaded MBs.

The unique nature of the MBs containing the Flu-CPAA-100 was conveyed in the acoustic studies where the backscattering enhancement and cavitation stability of the different MBs were monitored (Figs. 4 and 5). All MBs, except those containing Flu-CPAA-100, showed similar US enhancement (12–18 dB) and similar stability. This indicates a different MB assembly which leads to weakening of the MBs wall and makes it more susceptible to US mediated destruction (Eisenbrey et al., 2010b). However, acoustic enhancement is also diminished in this case.

The cytotoxicity of the SPF, which was assessed after MB insonation, revealed that those SPF containing Flu-CPAA-20 were less cytotoxic than those containing Flu-CPAA-100. Conjugating VRPMPLQ to the polymeric backbone of Flu-CPAA decreased its cytotoxicity (improved the viability of all three cell lines tested) (Fig. 7). This reduced cytotoxicity could be attributed to the lesser positive charge of the SPF containing the Flu-CPAA-Pep. Polycations aggregate on the cell surface compelled by their negatively charged membrane. The reduced cytotoxicity of the SPF containing polymers with VRPMPLQ may be explained by either reduction in the overall cationic charge of the Flu-CPAA-Pep products or by steric hindrance interfering with the polymer attachment to the negatively charged surface of the cells. These assumptions are supported by previous publications where decreasing the positive charge of polyethyleneimine, reduced its cytotoxicity (Lv et al., 2006; Yu et al., 2009; Zintchenko et al., 2008).

The cell-specific binding of the various Flu-CPAA products (excluding Flu-CPAA-100 that was found to be highly cytotoxic), before and after SPF production (Fig. 8), may be concluded as follows: (a) as expected, VRPMPLQ increased the attachment of Flu-CPAA-20 to all cell types, (b) VRPMPLQ increased the attachment of Flu-CPAA-100 to most cell types and (c) in general, SPF production improved cell binding. These observations are consistent with the fact that shattering a microbubble into small fragments will expose a large number of surface-exposed Flu-CPAA, which then becomes available for binding. Based on these cell-line studies it was decided to conduct the *in vivo* studies with DMH induced rats with SPF containing Flu-CPAA-Pep. The *in vivo* experiment protocols comprised rectal or IV administration of Flu-CPAA-20 and Flu-CPAA-100, with and without VRPMPLQ conjugate. The polymers were tested as is, or in SPF.

The low cytotoxicity and improved binding to colon cancer cells (Figs. 7 and 8) indicate that Flu-CPAA-20-Pep and Flu-CPAA-100-Pep as is or in SPF, are the optimal products along with the study objectives. Inasmuch, all polymers containing VRPMPLQ were superior in identifying malignant regions in the rat colons, after either IV or rectal administrations, due to enhanced binding to the mucosal tissues. Differences in the mucosal binding properties were observed among the polymers that did not contain peptide conjugate, depending on the mode of administration. While Flu-CPAA-20 (whether free or in SPF) attached similarly to the tissues after both IV and rectal administrations, Flu-CPAA-100 behaved

differently. Its tissue adherence was significantly ( $p = 0.008$ ) better after IV administration than after rectal administration when polymer-loaded SPF were used. The tissue binding of the free Flu-CPAA-100 was significantly better ( $p = 0.0007$ ) after rectal administration (Fig. 9). This dissimilarity could be explained by the high positive charge density of the Flu-CPAA-100. It caused this type of polymer to bind better to blood proteins when administered intravenously in its free form. When administered as SPF the PLA shielded the Flu-CPAA-100, leading to a higher amount of charged polymer to arrive at the target colonic tissue. It has been already pointed out that MBs can facilitate longer circulation time of the incorporated cargo by protecting them from the biological milieu (Sirsi et al., 2012).

Histological analysis of those malignant colon regions with highest levels of fluorescence revealed that they were dysplastic (Table 2), a finding which is supported by Miller et al. who found that VRPMPQLQ binds to a variety of unique targets on the surface of dysplastic cells (Miller et al., 2011). This property of affinity peptides to bind to malignant tissues at their dysplastic stage (Li et al., 2010) is encouraging and suggests that our approach could, indeed, be used for early detection of colon cancer. Currently, we are verifying the VRPMPQLQ specificity by a series of competitive studies in colon cancer cell lines and analyzing the role of linker length, used to anchor the peptide to the CPAA, on the recognition reaction efficiency.

## 5. Conclusion

We have shown that CPAA polymers bound preferentially to malignant regions in the rat colon after IV and rectal administrations. The addition of a recognition peptide, such as VRPMPQLQ, to the polymer backbone improved the preferential binding. The attachment of the peptide to the Flu-CPAA products also reduced the cytotoxicity of these cationic polymers. MBs did not affect the stability and the recognition capabilities of their CPAA product cargos even after US triggered production of SPF. It is speculated that loading the CPAA polymers into the MBs will protect them from premature interactions while circulating in the blood stream before reaching the target site, after IV administration. This entrapment would also increase the fraction that would bind to the malignant regions after local MBs disruption caused by directed US.

## Acknowledgements

The work was supported by a joint research grant from Drexel and HU-IDR and by a research grant from the Alex Grass foundation for Medicinal Chemistry. The authors would like to acknowledge the skillful work of Mr. Mordechai Goldminz and Ms. Gefen Amit. Abraham Rubinstein and Eylon Yavin are affiliated with David R. Bloom Center of Pharmacy.

## References

- Amri, R., Bordeianou, L.G., Sylla, P., Berger, D.L., 2013. Impact of screening colonoscopy on outcomes in colon cancer surgery. *JAMA Surg.* 1–7.
- Anderson, C.R., Hu, X., Zhang, H., Tlaxca, J., Declèves, A.E., Houghtaling, R., Sharma, K., Lawrence, M., Ferrara, K.W., Rychak, J.J., 2011. Ultrasound molecular imaging of tumor angiogenesis with an integrin targeted microbubble contrast agent. *Invest. Radiol.* 46, 215–224.
- Azab, A.K., Kleinstern, J., Srebnik, M., Rubinstein, A., 2008. The metastatic stage-dependent mucosal expression of sialic acid is a potential marker for targeting colon cancer with cationic polymers. *Pharm. Res.* 25, 379–386.
- Bloch, M., Kam, Y., Yavin, E., Moradov, D., Nissan, A., Ariel, I., Rubinstein, A., 2012. The relative roles of charge and a recognition peptide in luminal targeting of colorectal cancer by fluorescent polyacrylamide. *Eur. J. Pharm. Sci.* 47, 904–913.
- Borden, M.A., Zhang, H., Gillies, R.J., Dayton, P.A., Ferrara, K.W., 2008. A stimulus-responsive contrast agent for ultrasound molecular imaging. *Biomaterials* 29, 597–606.
- Bouakaz, A., Versluis, M., de Jong, N., 2005. High-speed optical observations of contrast agent destruction. *Ultrasound Med. Biol.* 31, 391–399.
- Cochran, M.C., Eisenbrey, J., Ouma, R.O., Soulen, M., Wheatley, M.A., 2011. Doxorubicin and paclitaxel loaded microbubbles for ultrasound triggered drug delivery. *Int. J. Pharm.* 414, 161–170.
- Duffy, M.J., 2001. Carcinoembryonic antigen as a marker for colorectal cancer: is it clinically useful? *Clin. Chem.* 47, 624–630.
- Edwards, B.K., Ward, E., Kohler, B.A., Ehemann, C., Zauber, A.G., Anderson, R.N., Jemal, A., Schymura, M.J., Lansdorp-Vogelaar, I., Seeff, L.C., van Ballegooijen, M., Goede, S.L., Ries, L.A., 2010. Annual report to the nation on the status of cancer, 1975–2006, featuring colorectal cancer trends and impact of interventions (risk factors, screening, and treatment) to reduce future rates. *Cancer* 116, 544–573.
- Eisenbrey, J.R., Burstein, O.M., Kambhampati, R., Forsberg, F., Liu, J.B., Wheatley, M. A., 2010a. Development and optimization of a doxorubicin loaded poly(lactic acid) contrast agent for ultrasound directed drug delivery. *J. Control. Release* 143, 38–44.
- Eisenbrey, J.R., Soulen, M.C., Wheatley, M.A., 2010b. Delivery of encapsulated doxorubicin by ultrasound-mediated size reduction of drug-loaded polymer contrast agents. *IEEE Trans. Bio-med. Eng.* 57, 24–28.
- Elwell, M.R., McConnell, E.E., 1990. Small and large intestine. In: Boorman, G.A., Eustis, S.L., Elwell, M.R., Montgomery, C.A.J., MacKenzie, W.F. (Eds.), *Pathology of the Fischer Rat: Reference and Atlas*. Academic Press, San Diego, USA, pp. 43–61.
- Endo-Takahashi, Y., Negishi, Y., Kato, Y., Suzuki, R., Maruyama, K., Aramaki, Y., 2012. Efficient siRNA delivery using novel siRNA-loaded bubble liposomes and ultrasound. *Int. J. Pharm.* 422, 504–509.
- Ferrara, K., Pollard, R., Borden, M., 2007. Ultrasound microbubble contrast agents: fundamentals and application to gene and drug delivery. *Annu. Rev. Biomed. Eng.* 9, 415–447.
- Gao, Z., Kennedy, A.M., Christensen, D.A., Rapoport, N.Y., 2008. Drug-loaded nano/microbubbles for combining ultrasonography and targeted chemotherapy. *Ultrasonics* 48, 260–270.
- Goetz, M., Ziebart, A., Foersch, S., Vieth, M., Waldner, M.J., Delaney, P., Galle, P.X., Neurath, M.F., Kiesslich, R., 2010. In vivo molecular imaging of colorectal cancer with confocal endomicroscopy by targeting epidermal growth factor receptor. *Gastroenterology* 138, 435–446.
- Hansen, M.B., Nielsen, S.E., Berg, K., 1989. Re-examination and further development of a precise and rapid dye method for measuring cell growing/cell kill. *J. Immunol. Methods* 119, 203–210.
- Hernot, S., Klibanov, A.L., 2008. Microbubbles in ultrasound-triggered drug and gene delivery. *Adv. Drug Deliv. Rev.* 60, 1153–1166.
- Hsiung, P.L., Hardy, J., Friedland, S., Soetikno, R., Du, C.B., Wu, A.P., Sahbaie, P., Crawford, J.M., Lowe, A.W., Contag, C.H., Wang, T.D., 2008. Detection of colonic dysplasia in vivo using a targeted heptapeptide and confocal microendoscopy. *Nat. Med.* 14, 454–458.
- Janakiram, N.B., Rao, C.V., 2008. Molecular markers and targets for colorectal cancer prevention. *Acta Pharm. Sin.* 29, 1–20.
- Jemal, A., Siegel, R., Xu, J., Ward, E., 2010. Cancer statistics. *CA: Cancer J. Clin.* 60, 277–300.
- Klibanov, A.L., 1999. Targeted delivery of gas-filled microspheres, contrast agents for ultrasound imaging. *Adv. Drug Deliv. Rev.* 37, 139–157.
- Kwon, Y.S., Cho, Y.S., Yoon, T.J., Kim, H.S., Choi, M.G., 2012. Recent advances in targeted endoscopic imaging: Early detection of gastrointestinal neoplasms. *World J. Gastrointest. Endosc.* 4, 57–64.
- LaMont, J.T., O'Gorman, T.A., 1978. Experimental colon cancer. *Gastroenterology* 75, 1157–1169.
- Lee, H., Jeong, J.H., Park, T.G., 2002. PEG grafted polylysine with fusogenic peptide for gene delivery: high transfection efficiency with low cytotoxicity. *J. Control. Release* 79, 283–291.
- Lentacker, I., De Geest, B.G., Vandenbroucke, R.E., Peeters, L., Demeester, J., De Smedt, S.C., Sanders, N.N., 2006. Ultrasound-responsive polymer-coated microbubbles that bind and protect DNA. *Langmuir* 22, 7273–7278.
- Li, M., Anastassiades, C.P., Joshi, B., Komarck, C.M., Piraka, C., Elmunzer, B.J., Turgeon, D.K., Johnson, T.D., Appelman, H., Beer, D.G., Wang, T.D., 2010. Affinity peptide for targeted detection of dysplasia in Barrett's esophagus. *Gastroenterology* 139, 1472–1480.
- Liu, J., Sun, Y.Q., Wang, P., Zhang, J., Guo, W., 2013. Construction of NIR and ratiometric fluorescent probe for Hg<sup>2+</sup> based on a rhodamine-inspired dye platform. *Analyst* 138, 2654–2660.
- Lv, H., Zhang, S., Wang, B., Cui, S., Yan, J., 2006. Toxicity of cationic lipids and cationic polymers in gene delivery. *J. Control. Release* 114, 100–109.
- Martinez-Rivas, A., Chinea, P., Favre, G., Pinaud, S., Séverac, C., Faye, J.C., Vieu, C., 2010. Detection of label-free cancer biomarkers using nickel nanoislands and quartz crystal microbalance. *Int. J. Nanomed.* 5, 661–668.
- Miller, S.J., Joshi, B.P., Feng, Y., Gaustad, A., Fearon, E.R., Wang, T.D., 2011. In vivo fluorescence-based endoscopic detection of colon dysplasia in the mouse using a novel peptide probe. *PLoS One* 6, e17384.
- Newberne, P.M., Rogers, A.E., 1985. Adenocarcinoma, colon and rectum, rat. In: Jones, T.C., Mohr, U., Hunt, R.D. (Eds.), *Monographs on Pathology of Laboratory Animals. Digestive System*. Springer, Heidelberg, Germany, pp. 365–370.
- Nicolau, C., Ripolles, T., 2012. Contrast-enhanced ultrasound in abdominal imaging. *Abdom. Imaging* 37, 1–19.
- Qin, S., Caskey, C.F., Ferrara, K.W., 2009. Ultrasound contrast microbubbles in imaging and therapy: physical principles and engineering. *Phys. Med. Biol.* 54, R27–R57.

- Quaia, E., 2007. Microbubble ultrasound contrast agents: an update. *Eur. Radiol.* 17, 1995–2008.
- Sirsi, S., Borden, M., 2009. Microbubble compositions, properties and biomedical applications. *Bubble Sci. Eng. Technol.* 1, 3–17.
- Sirsi, S.R., Hernandez, S.L., Zielinski, L., Blomback, H., Koubaa, A., Synder, M., Homma, S., Kandel, J.J., Yamashiro, D.J., Borden, M.A., 2012. Polyplex-microbubble hybrids for ultrasound-guided plasmid DNA delivery to solid tumors. *J. Control. Release* 157, 224–234.
- Tonini, G., Schiavon, G., Vincenzi, B., Santini, D., 2007. New target agents in the treatment of colorectal cancer. *Expert Opin. Drug Discov.* 2, 861–871.
- Whiteley, L.O., Anver, M.R., Bolts, S., Jokinen, M.P., 1994. Proliferative Lesions of the Rat Intestine. STP/ARP/AFIP, Washington.
- Xu, J.S., Huang, J., Qin, R., Hinkle, G.H., Povoski, S.P., Martin, E.W., Xu, R.X., 2010. Synthesizing and binding dual-mode poly(lactic-co-glycolic acid) (PLGA) nanobubbles for cancer targeting and imaging. *Biomaterials* 31, 1716–1722.
- Yu, J.H., Quan, J.S., Huang, J., Wang, C.Y., Sun, B., Nah, J.W., Cho, M.H., Cho, C.S., 2009. Alpha,beta-poly(L-aspartate-graft-PEI): a pseudo-branched PEI as a gene carrier with low toxicity and high transfection efficiency. *Acta Biomater.* 5, 2485–2494.
- Zhao, Y.Z., Du, L.N., Lu, C.T., Jin, Y.G., Ge, S.P., 2013. Potential and problems in ultrasound-responsive drug delivery systems. *Int. J. Nanomed.* 8, 1621–1633.
- Zintchenko, A., Philipp, A., Dehshahri, A., Wagner, E., 2008. Simple modifications of branched PEI lead to highly efficient siRNA carriers with low toxicity. *Bioconjugate Chem.* 19, 1448–1455.